

GaussianDWM: 3D Gaussian Driving World Model for Unified Scene Understanding and Multi-Modal Generation

Tianchen Deng^{1*}, Xuefeng Chen^{2*}, Yi Chen^{1*}, Qu Chen^{3,4}, Yuyao Xu^{3,4}, Lijin Yang^{3,4}, Le Xu^{3,4}, Yu Zhang^{3,4}, Bo Zhang^{3,4}, Wuxiong Huang^{3,4}, Hesheng Wang¹

¹ Shanghai Jiao Tong University ² Tsinghua University ³ MEGVII Technology ⁴ Mach Drive

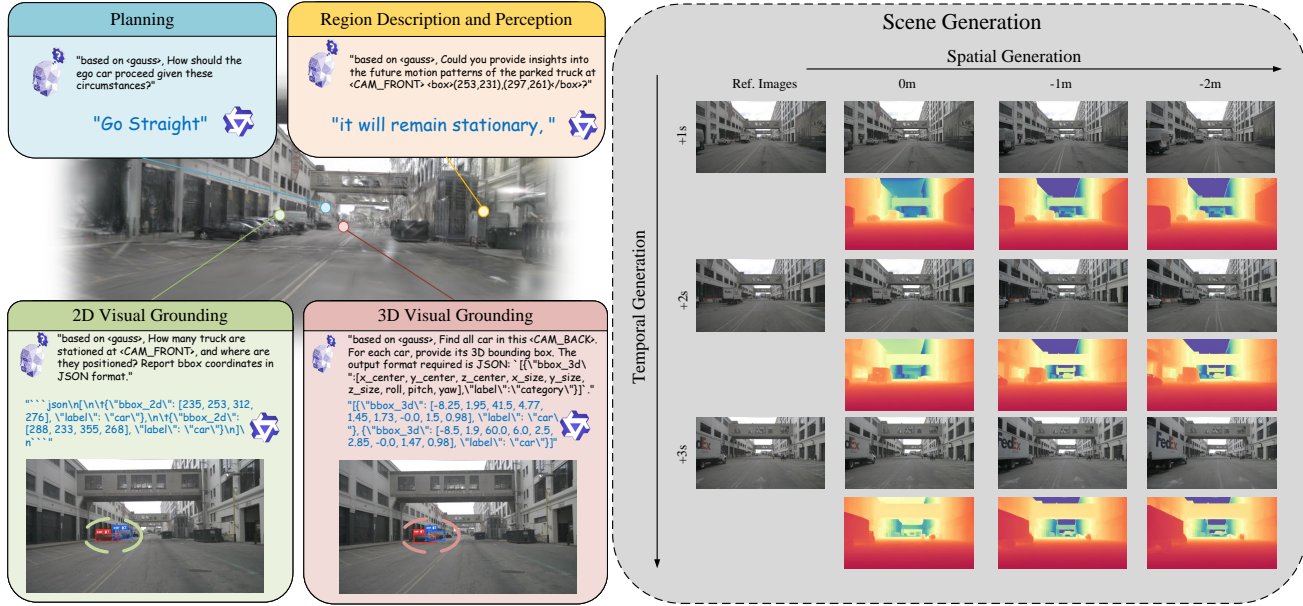


Figure 1. We propose the first unified 3D Gaussian-based world model framework that achieves comprehensive scene understanding and scene generation for driving scenarios. It efficiently encodes complex scenes, samples task-relevant information, and handles diverse question-answering tasks. Moreover, by leveraging the extracted world knowledge, our framework guides the generative model to perform accurate spatial and temporal scene generation.

Abstract

Driving World Models (DWMs) have been developing rapidly with the advances of generative models. However, existing DWMs lack 3D scene understanding capabilities and can only generate content conditioned on input data, without the ability to interpret or reason about the driving environment. Moreover, current approaches represent 3D spatial information with point cloud or BEV features do not accurately align textual information with the underlying 3D scene. To address these limitations, we propose a novel unified DWM framework based on 3D Gaussian scene representation, which enables both 3D scene understanding and multi-modal scene generation, while also enabling

contextual enrichment for understanding and generation tasks. Our approach directly aligns textual information with the 3D scene by embedding rich linguistic features into each Gaussian primitive, thereby achieving early modality alignment. In addition, we design a novel task-aware language-guided sampling strategy that removes redundant 3D Gaussians and injects accurate and compact 3D tokens into LLM. Furthermore, we design a dual-condition multi-modal generation model, where the information captured by our vision-language model is leveraged as a high-level language condition in combination with a low-level image condition, jointly guiding the multi-modal generation process. We conduct comprehensive studies on the nuScenes, and NuInteract datasets to validate the effectiveness of our framework. Our method achieves state-of-the-art performance. We will release the code publicly on

The first three authors contribute equally to this paper. Project leader: Qu Chen, Corresponding author: Hesheng Wang

1. Introduction

Driving World Model (DWM) [17, 23, 47] have become essential for autonomous driving for their ability to predict future scene generation. These models predict environmental changes and synthesize simulation data for risk forecasting, route optimization, and corner case training. Most existing approaches achieve this by predicting modalities such as images [60] and point clouds [59], which represent the visual and geometric properties of the environment. While these DWMs excel at forecasting how the environment may evolve, they are difficult to interpret, describe, or query, and cannot easily provide contextual information (e.g., visual question answering or scene description). With the rapid progress of Vision-Language Models (VLMs) [55], remarkable advancements have been achieved in general vision tasks by leveraging world knowledge and causal reasoning. This highlights the potential of combining the scene understanding capability of VLMs with the generative power of DWMs as a promising future direction. A recent pioneering effort in this direction is HERMES [64]. It adopts BEV features to represent spatial information, aligns them with the text space, and incorporates them into the generative model. However, this BEV-based scene representation only achieves feature-level alignment between textual and spatial inputs, which is not sufficiently accurate. To overcome this limitation, we propose a novel 3DGS-based scene representation that unifies scene understanding and generation.

First, we directly embed linguistic features into the 3D Gaussians, thereby achieving explicit spatial alignment between text and the 3D scene. This improves the accuracy of cross-modal alignment. Second, given the redundancy of Gaussians (i.e., extremely dense representations with tens of thousands of tokens per scene), it is impractical for VLMs to process such a large number of tokens effectively. To address this, we introduce a novel task-aware language-guided sampling strategy. By constructing cross-attention between the input text and the 3D Gaussians, our method selects the most relevant Gaussians for the query and projects them into the context space through our projector, injecting accurate and compact 3D tokens into the textual understanding. Finally, we design a dual-condition multi-modal generation model. In this framework, the understanding from the VLM provides a high-level language condition, while image features serve as a low-level image condition. Together, they guide the generation of multiple modalities, including RGB, depth, and language. Moreover, our framework supports both spatial and temporal generation. Overall, our contributions are shown as follows:

- We propose the first 3D Gaussian-based unified world model framework that supports both scene understanding

and scene generation.

- We introduce a novel token extraction and projection module for 3D Gaussian scene representations. Due to the redundancy of 3D Gaussians, we further develop a task-aware language-guided sampling strategy that overcomes token length limitations while preserving essential spatial information.
- We design a novel dual-condition multi-modal scene generation framework with high-level feature from world knowledge and low-level feature from images.
- Extended experiments on the Nuscenes and NuInteract datasets demonstrate that our method effectively bridges the gap between understanding and generation, enabling both accurate scene comprehension and more coherent future scene prediction.

2. Related Work

Novel View Synthesis for Urban Scene With the emergence of NeRF [35] and 3D Gaussian Splatting (3DGS) [25], many methods have adopted these representations across a wide range of tasks, including robotic mapping and localization [9, 11, 12, 14], VR [13, 18, 29], and autonomous driving [5, 36]. Early NeRF-based methods such as NSG [36], SUDS [43], ProSGN-eRF [8], EmerNeRF [56], and FreeDriveRF [49] achieved dynamic–static disentangled reconstruction through the use of scene graphs, optical flow, or other motion cues. More recently, several 3DGS-based approaches have been proposed to further improve rendering efficiency. PVG [4] introduces periodic vibration-based temporal dynamics to unify static and dynamic elements without manual annotations. Methods such as Street Gaussians [54], Driving Gaussian [63], and DeSiRe-GS [39] also explicitly separate dynamic and static components for reconstruction. LESSON [38] proposes a teacher-guided diffusion strategy for generating 3D Gaussian splats using only 2D supervision. STORM [57] proposes a feed-forward Transformer architecture to infer dynamic Gaussians and their velocities, enabling efficient large-scale outdoor scene reconstruction. DrivingForward [42] achieves feed-forward reconstruction from sparse surround-view inputs using self-supervised pose and depth estimation. MUDG [65] and Dist-4D [20] propose multi-modal novel view synthesis frameworks that generate both RGB and depth modalities.

Driving World Model Driving world models [27, 53] have attracted considerable attention in autonomous driving due to their ability to provide comprehensive environmental representations and predict future scenarios. Current methods primarily rely on 2D and 3D conditions for scene generation. GAIA-1 [24] introduces an autoregressive model for video generation in driving scenarios. DriveDreamer [60] proposes a scene generation framework conditioned on 3D structure to provide geometric representations that benefit

downstream autonomous driving tasks. MagicDrive [16] presents a street-view synthesis framework with precise 3D controls (e.g., camera poses, road maps) using cross-view attention, improving 3D object detection and BEV segmentation. DreamDrive [34] further combines video diffusion with hybrid Gaussian scene representations to synthesize 4D scenes with 3D-consistent dynamic video rendering. Most recently, UniScene [28] proposes an occupancy-centric approach that unifies semantic, visual, and LiDAR data generation. However, existing DWMs overlook the scene understanding ability of the driving environment.

Large Language Models for Driving Large Language Models (LLMs) have demonstrated impressive generalization ability and extensive world knowledge across various tasks, including scene understanding [22, 48, 62], visual question answering (VQA), and both 2D and 3D visual grounding. DriveGPT4 [52] processes front-view video inputs to predict vehicle actions while providing natural language justifications via an LLM. DriveLM [41] leverages LLMs for graph-based VQA and end-to-end autonomous driving. NuInteract [61] further integrates large vision-language models (LVLMs) with a spatial processor using a set of learnable queries, trained on the large-scale NuInteract dataset containing over 1.5M multi-view image-language pairs, covering dense scene captioning and diverse interactive tasks. GaussianVLM [21] introduces a 3D Gaussian-based visual question answering (VQA) framework, where a SceneSplat-style variational autoencoder (VAE) is employed to directly encode 3D Gaussian scenes. Hermes [64] proposes a BEV-based world model that integrates scene representation with a Vision-Language Model (VLM) for joint scene understanding and generation, which is the most closely related work to ours. However, existing approaches typically rely on image, point cloud, or BEV representations. In contrast, our method leverages a 3D Gaussian scene representation [10] that achieves explicit spatial alignment between language features and 3D geometry, resulting in more accurate multimodal correspondence and improved representation of both texture and structural information in complex environments.

3. Method

In this paper, we propose GaussianDWM, a unified framework with 3D gaussian scene representation for driving scenarios understanding and generation. The pipeline of our method is illustrated in Fig. 2. The input to our method consists of images $\{I_i\}$, Gaussian ellipsoids $\{G_i\}$, and query text $\{t_i\}$. The framework is composed of three main modules: (i) World tokenizer (Sec. 3.1); (ii) Scene Understanding (Sec. 3.2); (iii) Multi-modal Generation (Sec. 3.3). We elaborate on the entire pipeline of our system in the following subsections.

3.1. World Tokenizer

Our world tokenizer encodes the world observations, i.e., the current multi-view images, into a compact continuous 3D Gaussian representation. We then apply a gaussian projector to align the selected 3D features to the text space before processing by the VLM.

3D Gaussian Tokenizer To preserve texture, 3D structure, and language alignment, we adopt 3D Gaussians as the scene representation for LLM input. We build upon LangSplat [40] to construct a 3DGS language field, where each Gaussian is augmented with a language embedding f_i . These embeddings are obtained from CLIP features, which inherit hierarchical semantics extracted via SAM [26]. We then follow the standard 3DGS rendering strategy, incorporating language information directly into the Gaussian primitives.

$$\mathbf{F}(v) = \sum_{i \in \mathcal{N}} f_i \alpha_i \prod_{j=1}^{i-1} (1 - \alpha_j) \quad (1)$$

where $\mathbf{F}(v)$ represents the language embedding rendered at pixel v , and $\alpha_i = o_i G_i^{2D}(v)$. Here o_i is the opacity of the i th Gaussian and $G_i^{2D}(\cdot)$ represents the function of the i -th Gaussian projected onto 2D. To further reduce memory consumption and improve efficiency, we introduce a scene-wise language autoencoder E , which maps the CLIP embeddings $\mathbf{F}(v) \in \mathbb{R}^D$ to $\mathbf{H}(v) = E(\mathbf{F}(v)) \in \mathbb{R}^d$, where $d \ll D$. We select $d = 3, D = 512$. Then we learn a decoder Ψ to reconstruction CLIP feature. Our autoencoder can significantly decrease memory requirements while retaining semantic fidelity.

3D Gaussian Projector We first align the extracted 3D Gaussian tokens to the text space. For each Gaussian primitive G_i , we represent its attributes as $G_i = (x_i, o_i, s_i, r_i, f_i)$ where $x_i \in \mathbb{R}^3$ denotes the 3D spatial position, o_i the opacity, s_i the scale, r_i the rotation, and f_i the associated CLIP feature. For the Gaussian tokenizer, we first apply learnable Fourier embeddings [35] to the 3D coordinates x_i :

$$\gamma(x_i) = [\sin(2^k \pi x_i), \cos(2^k \pi x_i)]_{k=0}^{L-1}, \quad (2)$$

where L is set to 10. For the opacity o_i , we apply a sigmoid activation $\hat{o}_i = \sigma(o_i)$ to constrain the value to $[0, 1]$. For the CLIP feature f_i , we use a pre-trained scene-wise decoder to project it to a 512 dimension $\tilde{f}_i = \Psi(f_i) \in \mathbb{R}^{N \times 512}$. N denotes the number of 3D Gaussian ellipsoids. Then, we employ a set of MLP projectors to map Gaussian attribute into a shared 4096-dimensional feature space, i.e., $h_i^x = \phi_x(\gamma(x_i))$, $h_i^o = \phi_o(\hat{o}_i)$, $h_i^s = \phi_s(s_i)$, $h_i^r = \phi_r(r_i)$, and $h_i^f = \phi_f(\tilde{f}_i)$, where $\gamma(\cdot)$ is the Fourier embedding and each $\phi(\cdot)$ is a learnable MLP. Finally, we fuse the projected features via learnable weights to obtain the Gaussian scene token $\mathcal{G}_i = \sum_{p \in \{x, o, s, r, f\}} \alpha_p \cdot h_i^p$, where each α_p is a trainable scalar normalized by a softmax. For text queries, we

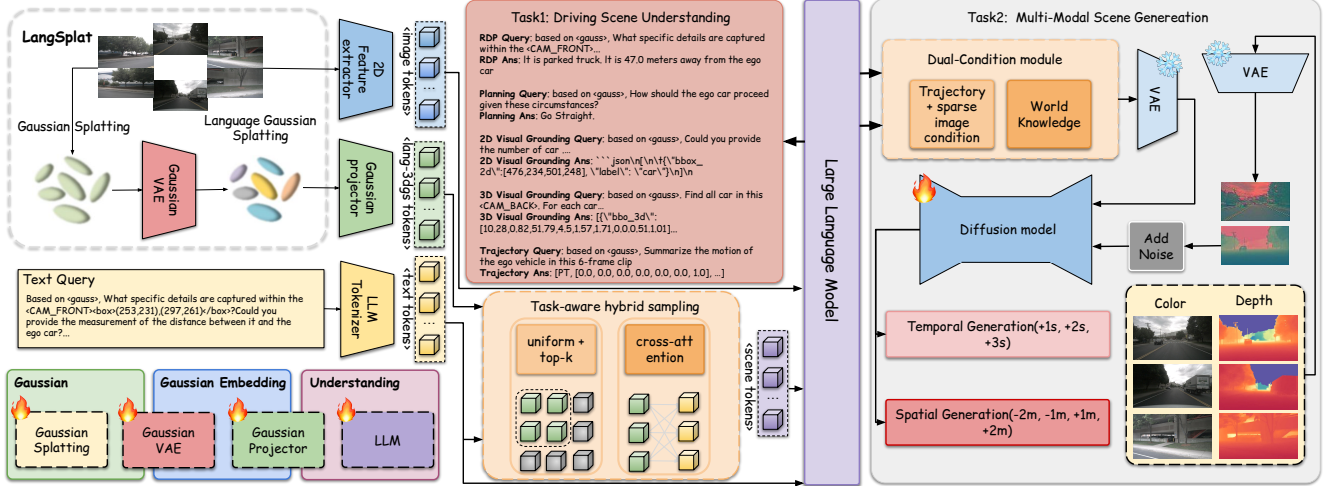


Figure 2. **System Overview.** We propose the first unified 3D Gaussian-based world model framework that simultaneously supports both scene understanding and scene generation. We first employ a scene encoder to align the language information with the 3D Gaussians, resulting in language-augmented 3D Gaussian representations. Then, a designed Gaussian projector aligns the 3D Gaussian tokens, 2D image tokens, and text tokens into a unified latent space. Subsequently, a task-aware hybrid sampling strategy is applied to select the most relevant 3D Gaussian tokens for the current query, which are then fed into the LLM. The LLM produces both textual answers and high-level language features that encapsulate world knowledge, which are later used to guide multi-modal scene generation.

tokenize the input prompts into vocabulary indices and text tokens \mathcal{T} for LLM processing.

3.2. Scene Understanding

This section introduces the world understanding module. The Large Language Model (LLM) interprets driving scenarios from the world tokenizer outputs $\mathcal{G}_i \in \mathbb{R}^{N \times C}$ according to user instructions. Then, the LLM parses the user instruction \mathcal{T}_i and extracts world knowledge from the driving scene, generating both a textual answer t_i and a language feature representation C_L , which is later used as a condition signal for scene generation. This feature encodes high-level world knowledge as well as spatial information and is later used as a condition for scene generation. We implement the LLM using the widely adopted Qwen3 model [55]. The overall architecture is:

$$\{t_i, C_i^l\} = LLM(\mathcal{G}_i, \mathcal{T}_i) \quad (3)$$

Task-aware Language-guided Sampling However, directly converting all Gaussians into tokens would exceed the maximum token length limits of LLMs, and the high degree of redundancy in the Gaussian set would make it difficult for the LLM to reason about spatial interactions across different views. To address this, we propose a task-aware hybrid sampling strategy tailored for 3D Gaussian scene representations. For scene understanding tasks, we adopt a global sampling strategy that preserves holistic scene information by selecting a representative subset of Gaussians. We apply both uniform sampling and top-k sampling to select $N = 4096$ gaussian tokens from the hundreds of thou-

sands in the scene, which are then fed into the LLM. In contrast, for 2D and 3D visual grounding tasks, we further introduce a language-guided sampling module, which re-tokenizes the dense scene representation into a more compact and sparse form conditioned on the text query. Specifically, we apply cross-attention between the 3D Gaussian features and the text query to identify and retain only those Gaussians that are most relevant to the query. This design is highly effective for both 2D and 3D grounding tasks, as it enables the model to selectively inject the most relevant 3D spatial information into the language reasoning process. Compared with the previous Hermes framework, our 3D Gaussian-based LLM model can effectively respond to user queries about the driving environment, providing scene descriptions and answers to visual questions. In addition, it supports both 2D and 3D visual grounding tasks, achieving state-of-the-art performance.

Training Strategy Similarly to many VLM training protocols, we follow a two-stage training with alignment and fine-tuning phase. During the alignment phase we freeze the 3D backbone and LLM tokenizer, training the sparsifier modules and the transformer for textual alignment of the vision tokens. The LLM is adapted using LoRA. Both stages share a unified training objective. Following, we use a prefix language modeling, where the model is conditioned on an input prefix and trained to autoregressively generate the target continuation:

$$\mathcal{L}(\theta, \mathcal{B}) = - \sum_{\{t_{\text{prefix}}, t_{\text{gt}}\} \in \mathcal{B}} \sum_{i=1}^{|t_{\text{gt}}|} \log p_{\theta} \left(t_{\text{gt}}^{(i)} \mid t_{\text{gt}}^{(<i)}, t_{\text{prefix}} \right), \quad (4)$$

where θ are the model parameters, \mathcal{B} denotes a batch of samples of prefix input t_{prefix} (text tokens, image tokens and 3D Gaussian tokens), and ground truth response $t_{\text{gt}}, t_{\text{gt}}^{(t)}$ denotes the t -th token in the ground truth response sequence.

3.3. Multi-modal Scene Generation

In this section, we propose a dual condition multi-modal scene generation model. Our model consists a denoising UNet [2], and a frozen pre-trained VAE [50] to encode RGB images I_i , and depth maps D_i into a unified latent space. To satisfy the VAE input specifications, we convert depth maps into pseudo-RGB images via channel replication. The VAE encoding process can be written as: $z_I = \mathcal{E}(I_i)$, $z_D = \mathcal{E}(D_i)$. During decoding, the VAE decoder \mathcal{D} reconstructs RGB, and depth from the latent variable z_i . For the depth map, we average the three output channels of the decoded result to obtain the final single-channel depth prediction: $\hat{I}_i = \mathcal{D}(z_I)$, $\hat{D}_i = \frac{1}{3} \sum_{c=1}^3 \mathcal{D}(z_D)_c$. In the training phase, we random sample on the known camera trajectory, and get the latent code of corresponding color and depth images with the VAE encoder z_I, z_D . At each timestep t , we add noise to the sampled data. Then, we use the projection matrix to project surrounding point cloud at time t to time $t+n$ to serve as low-level image conditions $\{C_I, C_D\}$. Then we concatenate the noisy latent representations of each modality with the low-level image control signal and high-level language control signal C_L from LLM as the input to the denoising diffusion network. The model is using a v-prediction objective. The target \mathbf{v}_t is defined as: $\mathbf{v}_t = \alpha_t \epsilon_t - \sigma_t d_t$, where $\epsilon_t \sim \mathcal{N}(0, I)$ denotes the sampled gaussian noise, α_t and σ_t represent the time-dependent noise scheduling coefficients, and d_t corresponds to the noisy input modality requiring denoising. The training objective is defined as:

$$\mathcal{L} = \mathbb{E}_{d, \epsilon, t, s} \| \mathcal{F}_{\theta} (d_t, d_{\text{ref}}, C_I, C_D, C_L, s) - \mathbf{v}_t \|_2^2, \quad (5)$$

The low-level conditions C_I and C_D represent the scene's texture and geometric information, guiding the generation process. Meanwhile, the high-level language feature C_L encapsulates comprehensive world knowledge extracted from the LLM. By conditioning the generation on multiple levels of information, our model achieves more accurate and consistent temporal and spatial synthesis.

For spatial generation, we project the surrounding point cloud using the spatial transformation of the query frame to obtain a sparse condition map. For temporal generation, we utilize the trajectory predicted by the front-end LLM to

project the point cloud and construct a temporal sparse condition map, enabling temporally coherent scene generation.

Our generation model supports both spatial scene generation, i.e., novel view synthesis with spatial shifts of 1m or 2m, and temporal scene generation, i.e., future scene prediction at 1s and 2s into the future.

4. Experiments

4.1. Dataset and Evaluation Metric

We evaluate our method on two datasets for both scene understanding and scene generation. NuScenes [3] is a widely used autonomous driving dataset containing 700 training scenes, 150 validation scenes, and 150 test scenes. We use six surrounding camera images as inputs. NuInteract [61] are recent benchmark for scene understanding. NuInteract provides ~ 1.5 M annotations and supports multiple tasks, including 2D perception and 3D visual grounding. For scene understanding, we adopt standard language and captioning metrics, including gCIDEr [44], BLEU-4 [37], ROUGE [31]. For scene generation, we use FID for images, and FVD for videos as evaluation metrics.

4.2. Implementation Details

Our training pipeline consists of three stages. In the first stage, we train the Gaussian tokenizer, projector, and the proposed sampling strategy independently. We then integrate these components with the LLM and perform joint fine-tuning. For the LLM, we adopt a LoRA-based fine-tuning strategy. All models in this stage are trained using 16 NVIDIA A100 GPUs. In the second stage, we train the multi-modal generation module. We start by training a low-resolution (224×400) RGB video generation model, extend it to low-resolution RGB-D generation, and finally refine it into a high-resolution (424×800) RGB-D video generator using a mixed-frame-length strategy. The model is optimized using simulation-free rectified flow and a v-prediction loss [15]. In the final stage, we perform end-to-end joint optimization over all components to ensure consistency between scene understanding and scene generation.

4.3. Scene Understanding

In this section, we present the results of **scene understanding**, which are divided into four tasks: region description and perception, planning, 2D visual grounding, and 3D visual grounding. The results are shown in Tab. 1. The experimental settings strictly follow Drivemonkey [61]. We primarily compare two categories of methods: (1) LLM-based visual grounding approaches such as LLaVA [32] and InternVL [6], and (2) specialized 3D detection models such as BEVFormer [30], PETR [33], and CAPE [51]. As shown in Tab. 1, GaussianDWM significantly outperforms previous LVLMs in terms of average metrics across

Model	Years	LLM	2D RD & Pre ↑			2D VG ↑			3D VG ↑			Plan ↑	
			BLEU	Rouge_L	CIDEr	mAP	F1	MIoU	Pr	mAP	F1	Acc	Avg. ↑
LLaVA1.5	2024	Vicuna-7B	64.23	76.69	74.82	0.10	0.16	14.31	6.51	5.33	3.12	36.20	28.16
MiniCPM-V 2	2024	MiniCPM-2B	47.43	63.16	69.88	0.11	0.13	13.34	0.97	1.55	0.86	36.69	23.41
MiniCPM-V 2.6	2024	QWen2-7B	47.92	69.11	70.20	0.36	0.49	18.74	1.97	1.61	0.93	36.42	24.78
InternVL1.5-2B	2024	InternLM2-7B	67.14	81.10	79.83	14.74	17.64	55.43	28.05	21.73	12.92	53.96	43.25
InternVL1.5-4B	2024	Phi3-4B	66.63	80.64	79.24	14.27	17.60	53.52	25.14	19.46	11.63	40.25	40.84
QWen2VL	2024	Qwen2-2B	67.92	80.24	78.51	17.11	20.87	57.24	12.82	10.20	6.12	45.59	39.66
Qwen2VL	2024	Qwen2-7B	66.65	78.57	77.97	16.06	20.04	55.51	20.64	16.26	9.82	49.33	41.09
InternVL2-1B	2024	Qwen2-0.5B	66.89	81.00	79.59	16.70	20.21	55.94	23.36	18.35	10.94	44.08	41.71
InternVL2-2B	2024	InternLM2-2B	66.77	80.87	79.62	16.12	19.49	55.29	27.83	21.09	12.58	44.61	42.43
InternVL2-4B	2024	Phi3-4B	66.88	80.76	79.29	19.14	23.47	59.07	25.28	20.12	11.97	40.43	42.64
InternVL2-8B	2024	InternLM2.5-7B	67.32	81.39	80.01	<u>20.61</u>	<u>25.24</u>	<u>61.90</u>	31.47	24.67	14.70	46.93	45.42
DriveMonkey	2025	InternLM2.5-7B	67.50	81.15	79.79	19.47	24.02	59.36	51.90	<u>34.53</u>	20.86	82.64	<u>52.12</u>
Bevformer	2022	-								44.50	23.69	1.576	
PETR	2022	-								55.80	31.34	20.58	Unsupported
CAPE	2023	-								<u>55.02</u>	32.94	21.33	
GaussianDWM	2025	Qwen3-8B	66.17	79.07	77.06	34.95	40.49	71.85	50.66	52.78	32.05	<u>66.27</u>	57.14

Table 1. The comparison between our **GaussianDWM** and other state-of-the-art models on the NuInteract dataset [61]. The scene understanding task includes four subtasks: region description and perception, 2D visual grounding, 3D visual grounding, and planning. Our method achieves state-of-the-art results across all four tasks, which fully demonstrates the effectiveness of introducing a 3D Gaussian scene representation for enhancing the LLM’s capability to understand 3D spatial information.

Finetune	Gaussian	Sampling	2D RD & Pre ↑			2D VG↑			3D VG↑			Plan↑	
			BLEU	Rouge_L	CIDEr	mAP	F1	MIoU	Pr	mAP	F1	Acc	Avg.↑
zeroshot	w/o		2.91	12.68	0.59	0.00	0.00	12.24	48.75	47.59	29.12	0.00	15.39
finetuned	w/o		65.09	78.35	76.56	30.01	35.45	69.01	50.36	51.88	31.43	45.09	53.32
finetuned	w	Random	66.19	<u>79.00</u>	<u>76.97</u>	<u>33.94</u>	<u>39.37</u>	<u>71.40</u>	<u>50.94</u>	<u>52.85</u>	<u>32.03</u>	<u>49.43</u>	55.21
finetuned	w	Top-k + Uniform	<u>66.17</u>	79.07	77.06	33.89	39.31	71.37	51.16	52.87	32.05	66.27	<u>56.92</u>
finetuned	w	Top-k + Uniform + CrossAttn	-			34.95	40.49	71.85	50.66	52.78	32.05	-	-

Table 2. We conduct ablation studies to validate the effectiveness of each proposed component, including the 3D Gaussian scene representation, the top-k and uniform sampling strategies, and the cross-attention-based sampling module. Note that the cross-attention sampling strategy is applied only to grounding tasks requiring focused attention (e.g., 2DVG and 3DVG).

all tasks on the NuInteract test dataset. It achieves state-of-the-art results on the RDP, 2D VG, and 3D VG tasks, effectively demonstrating the importance of introducing a 3D Gaussian scene representation for enabling LLMs to better comprehend 3D spatial information. Compared with previous point cloud- and BEV-based scene representations, our 3D Gaussian formulation allows for explicit alignment between 3D structural, texture, and language features, leading to more efficient and semantically consistent information injection into LLMs. Moreover, our task-aware hybrid sampling strategy efficiently selects Gaussian tokens most relevant to the query text while filtering out redundant 3D Gaussians. Compared with the current state-of-the-art VQA method Drivemonkey, our model shows clear advantages in both 2D and 3D visual grounding tasks, while also achieving comparable performance to specialized 3D detectors designed specifically for 3D VG.

4.4. Scene Generation

In this section, we present the evaluation of multi-modal scene generation, which includes both spatial scene generation and temporal scene generation. All experiments are

conducted on the nuScenes dataset [3]. Following previous works [16, 20], we interpolate the 2Hz keyframe annotations to a higher frame rate of 12Hz, and the experimental settings strictly follow [20].

We compare our method with representative street-view synthesis approaches, including PVG [4], EmerNeRF [56], StreetGaussian [54], OmniRe [7], FreeVS [45], DiST-4D [19]. As shown in Tab. 3, our method outperforms all existing methods and achieves state-of-the-art performance. We use FID and FVD as evaluation metrics since ground-truth data is not available after spatial shifts. Our method demonstrates superior consistency and photorealism under extreme viewpoint shifts ($\pm 4m$), outperforming direct reconstruction-based approaches. This indicates that our framework effectively combines the advantages of 3D Gaussian scene representation and diffusion-based generative modeling. Under the guidance of our dual-condition mechanism—leveraging both high-level world knowledge and low-level geometric cues—our method achieves state-of-the-art spatial and texture fidelity under large viewpoint variations.

We also visualize the qualitative results of spatial scene

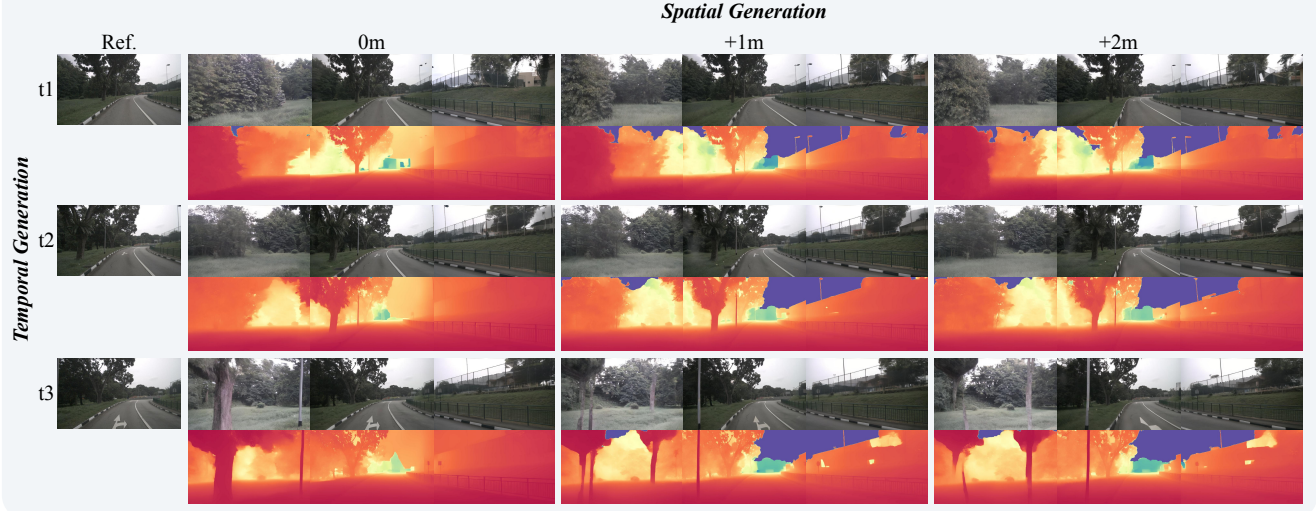
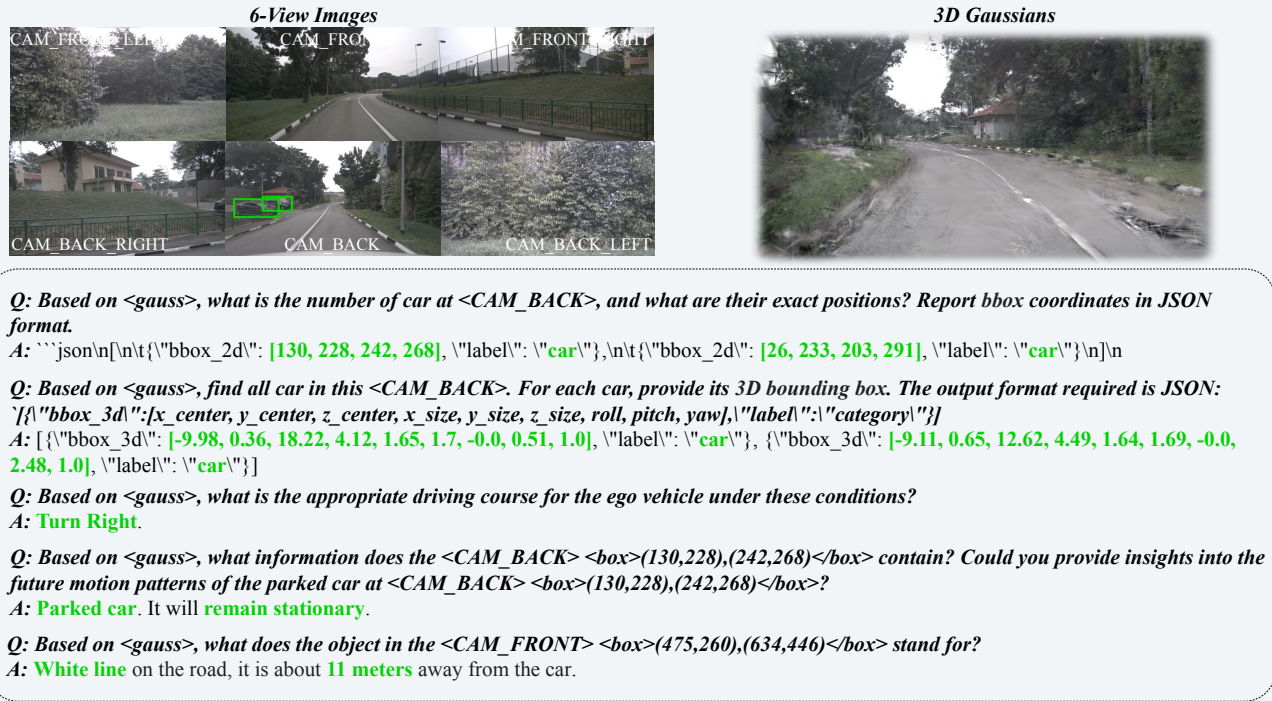


Figure 3. **Qualitative results for scene understanding and scene generation.** From top to bottom, we display the multi-view input of the current scene and the 3D Gaussian ellipsoids, the scene understanding results, and the spatial and temporal scene generation results.

generation in Fig. 3. We further compare our method with several existing novel view synthesis approaches, and the qualitative results are presented in Fig. 4. As shown, our RGB and depth generations exhibit photorealistic quality, demonstrating the complementary strengths of world knowledge, diffusion-based generation, and 3D Gaussian scene representation.

The proposed dual-condition design enables high-level world knowledge to effectively guide the model’s temporal reasoning for future scene prediction, while the low-

level sparse condition constrains 2D texture and style consistency. This demonstrates the importance of incorporating explicit **world knowledge** into world models to improve both semantic and spatial coherence during temporal generation. Overall, GaussianDWM is capable of simultaneously understanding and generating complex driving scenarios, highlighting a promising research direction toward unified scene understanding and generation in world modeling.

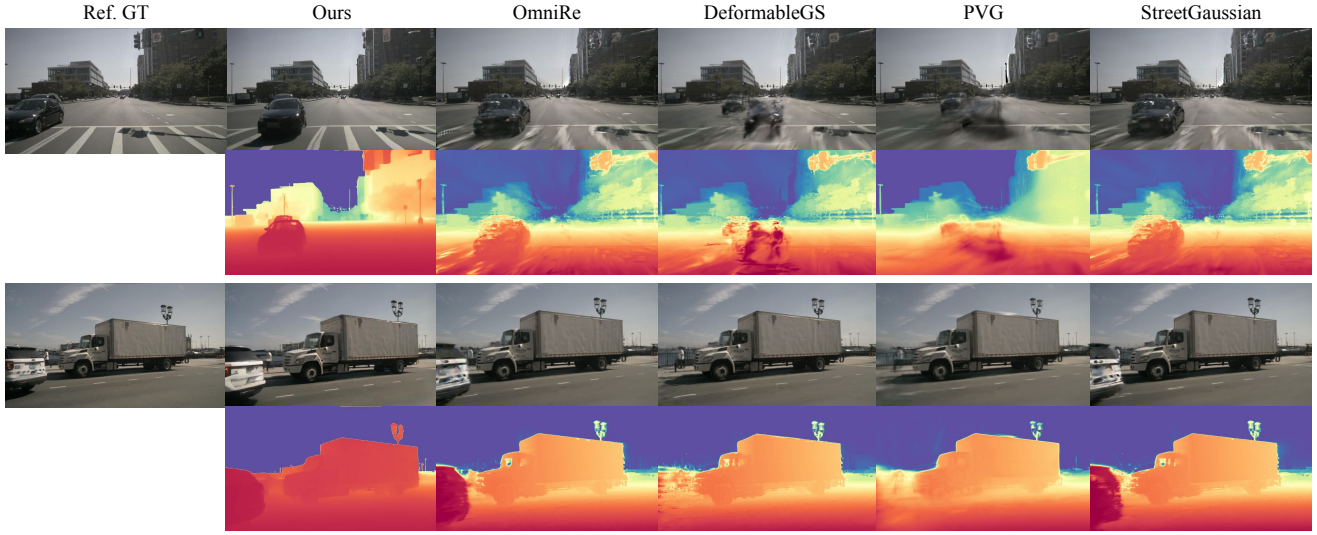


Figure 4. **Qualitative comparison of RGB-D NVS with 2m shift.** Compared with state-of-the-art reconstruction-based methods for spatial NVS [4, 7, 54, 58], our method reduce artifacts of dynamic objects and preserves temporal-spatial consistency across large viewpoint shifts.

Method	Shift ± 1		Shift ± 2		Shift ± 4	
	FID \downarrow	FVD \downarrow	FID \downarrow	FVD \downarrow	FID \downarrow	FVD \downarrow
PVG	48.15	246.74	60.44	356.23	84.50	501.16
EmerNeRF	37.57	171.47	52.03	294.55	76.11	497.85
StreetGaussian	32.12	153.45	43.24	256.91	67.44	429.98
OmniRe	31.48	152.01	43.31	254.52	67.36	428.20
FreeVS	51.26	431.99	62.04	497.37	77.14	556.14
DiST-S	10.12	45.14	12.97	68.80	17.57	105.29
Ours	8.36	44.50	11.27	68.17	18.81	116.40

Table 3. **Quantitive comparison** between our method and other novel view synthesis methods on nuScenes dataset.

4.5. Ablation Study

In this section, we conduct comprehensive ablation studies to validate the effectiveness of each component in our proposed framework. We systematically analyze the impact of the key modules, including the 3D Gaussian scene representation, the hybrid sampling strategies, and the dual-condition generation design, to demonstrate their respective contributions to the overall performance.

3D Gaussian Representation Compared with other scene representations, the 3D Gaussian scene representation provides a better ability to encode environmental features, including both texture and geometric information, and can be directly aligned to the 3D space through language features. The results are shown in Tab. 2. Through ablation studies, we fully verify that the introduction of 3D Gaussian representations enhances the LLM’s 3D scene understanding capability, enabling it to better perceive the geometric and semantic information of the scene.

Low-Level	High-level	FID $\pm 1m$	FID $\pm 2m$
✗	✓	-	-
✓	✗	10.12	45.14
✓	✓	8.36	44.5

Table 4. **Ablation Study of dual-condition generation mechanism.** “-” denotes failure under the setting.

Hybrid Sampling Based on the observed redundancy in the 3D Gaussian scene representation, we design a hybrid sampling strategy to extract the most informative components of the environment. The results are shown in Tab. 2. By comparing random sampling, uniform+top-k sampling, and cross-attention sampling, we observe that when cross-attention sampling is applied between the text query and the 3D Gaussian tokens, the model can more effectively select task-relevant Gaussian tokens, leading to improved scene understanding performance.

High-level World Knowledge Compared with other world model and scene generation frameworks, we design a dual-condition guidance framework that controls scene generation at different levels. The ablation results for this part are shown in Tab. 4. It can be observed that our method performs better in long-sequence prediction and under large viewpoint variance, demonstrating the effectiveness of incorporating world knowledge.

5. Conclusion

This paper introduces a novel unified driving world model framework that supports both scene understanding and generation within a single architecture. We bridge the gap

between these two tasks by proposing a new 3D Gaussian scene representation combined with a task-aware hybrid Gaussian sampling strategy, enabling effective world-query injection into the LLM. Extensive experiments validate the effectiveness of the proposed framework, demonstrating significant improvements in both scene understanding and generation. We believe this work an important step toward unified driving world models with 3D Gaussian scene representations.

Acknowledgement We sincerely thank Yikang Ding from Kuaishou Kling AI for his kind help and support.

A. Overview

In this supplementary material, we first provide additional details on constructing the 3DGS dataset from the large-scale nuScenes dataset, as well as the caption dataset used for trajectory prediction. We then describe the implementation and training details in Sec. C and Sec. D. Finally, in Sec. E, we present extensive experimental results across various datasets.

B. Dataset Details

To represent scenes from the NuScenes dataset [3] using 3D Gaussians, we construct the first large-scale 3D Gaussian dataset for outdoor urban environments, comprising 800 scenes derived from the original nuScenes sequences. Our goal is to build a dataset that enables generalizable 3D Gaussian-based scene understanding with LLMs, providing high-quality geometry and appearance representations suitable for downstream reasoning tasks.

Dataset Processing Many scenes contain frames with very low overlap or severe motion blur, making it difficult to obtain accurate 3DGS reconstructions. Therefore, we remove images or entire scenes whose reconstruction quality does not meet our standard. Since NuScenes dataset [3] provides high-quality LiDAR point clouds, we initialize each scene using aggregated LiDAR points, avoiding the large-scale inaccuracies that would arise from using COLMAP as in conventional 3DGS pipelines. For scenes with available depth supervision, we additionally apply a depth loss to improve geometric fidelity. After optimization, we further filter reconstructed scenes based on the PSNR metric before using them as inputs for our pre-training.

Language Label Collection and Training Our language label collection aims to establish 3D language paired data by associating each 3D Gaussian primitive with a rich language feature f_i . We build upon LangSplat [40] to construct a 3DGS language field. These embeddings are obtained from CLIP features, which inherit hierarchical semantics extracted via SAM [26]. We then follow the standard 3DGS rendering strategy, incorporating language information directly into the Gaussian primitives. As a collec-

tion of anisotropic 3D Gaussians, with each Gaussian $G(x)$ characterized by a mean $\mu \in \mathbb{R}^3$ and a covariance matrix Σ :

$$G(x) = \exp\left(-\frac{1}{2}(x - \mu)^\top \Sigma^{-1}(x - \mu)\right). \quad (6)$$

To optimize the parameters of 3D Gaussians, they are rendered into 2D image planes and a tile-based rasterizer is used to improve the rendering efficiency:

$$C(v) = \sum_{i \in \mathcal{N}} c_i \alpha_i \prod_{j=1}^{i-1} (1 - \alpha_j), \quad (7)$$

We also adopt the tilebased rasterizer to retain the rendering efficiency:

$$\mathbf{F}(v) = \sum_{i \in \mathcal{N}} f_i \alpha_i \prod_{j=1}^{i-1} (1 - \alpha_j) \quad (8)$$

where $\mathbf{F}(v)$ represents the language embedding rendered at pixel v , and $\alpha_i = o_i G_i^{2D}(v)$. Here o_i is the opacity of the i th Gaussian and $G_i^{2D}(\cdot)$ represents the function of the i -th Gaussian projected onto 2D.

For scene representation, each environment typically requires several million Gaussians to model its geometry and appearance. Since CLIP embeddings are high-dimensional features, directly learning the latent feature f_i for every Gaussian in the CLIP space would dramatically increase both memory consumption and computational cost—particularly because each f_i has a dimensionality of 512.

To further reduce memory consumption and improve efficiency, we introduce a scene-wise language autoencoder E , which maps the CLIP embeddings $\mathbf{F}(v) \in \mathbb{R}^D$ to $\mathbf{H}(v) = E(\mathbf{F}(v)) \in \mathbb{R}^d$, where $d \ll D$. We select $d = 3, D = 512$. The autoencoder is trained with a reconstruction objective on the CLIP embeddings. We also learn a decoder Ψ to reconstruct CLIP feature. Our autoencoder can significantly decrease memory requirements while retaining semantic fidelity.

$$\mathcal{L}_{ae} = \sum_{t=1}^T d_{ae} (\Psi(E(\mathbf{F}(v))), \mathbf{F}(v)), \quad (9)$$

After training the autoencoder, we transform all CLIP embeddings into scene-specific latent features $\mathbf{H}(v)$. We let our 3D language Gaussians learn language embeddings in the scene-specific latent space instead of the CLIP latent space. Compared to directly modeling the 512-dimensional CLIP embeddings, we significantly reduced the memory cost by incorporating scene priors. We optimized the language embeddings with the objective:

$$\mathcal{L}_{\text{lang}} = \sum_{l \in \{s, p, w\}} \sum_{t=1}^T d_{\text{lang}} (\mathbf{F}_t^l(v), \mathbf{H}_t^l(v)) \quad (10)$$

where $d_{\text{lang}}()$ denotes the distance function used for our 3D Language Gaussians. To inject the 3D Gaussian tokens into the query text input, we reconstruct a dedicated QA dataset. Moreover, to align with the training paradigm of QwenVL, all 3D Gaussian token annotations are placed at the beginning of each instruction. The exact formatting protocol is illustrated as follow:

```

1 {
2     "token": "fd8420396768425eabec9bddd7e64b6",
3     "scene_token": "e7ef871f77f44331aefdebc24ec034b
4         7",
5     "scene_idx": 2,
6     "frame_idx": 0,
7     "category": "2D_perception_infos",
8     "task": "rdp",
9     "conversations": [
10         {
11             "from": "human",
12             "value": "based on <gauss>, Can you quantify
13                 the distance separating the <CAM_FRONT>
14                 <box>(14,219),(37,248)</box> from the
15                 ego car?"
16         },
17     ],
18     "image": [
19         "nuscenes/samples/CAM_FRONT/n015-2018-08-02-17
20             -16-37+0800__CAM_FRONT__1533201470412460.
21             jpg"
22     ],
23     "views": ["CAM_FRONT"],
24     "gauss": [
25         "gauss/output-full-6v/2_CAM_FRONT/langsplat_3/
          per_frame/00000.pth"
26     ]
27 }
```

Trajectory Dataset Generation Our generative model supports both temporal and spatial scene generation. For spatial generation, text queries typically take the form “generate the view after shifting 2 m to the left.” In this case, we first use the LLM to infer the target camera pose. Using the predicted pose, we project the point cloud to obtain a sparse condition, which serves as the low-level guidance for the diffusion model.

For temporal generation, queries are typically phrased as “predict the scene 1 second later.” The LLM performs trajectory prediction and directly outputs the future camera pose. Based on this pose, we again apply point-cloud projection to generate the sparse condition used for temporal guidance.

To enable temporal scene generation, the LLM must possess the capability to predict future trajectories. Based on this requirement, we construct a trajectory-oriented QA dataset to supervise and enhance the model’s trajectory reasoning ability. From each video clip, we extract a 10-frame

sequence. The first 4 frames are provided to the model as the prompt input, while the remaining 6 frames are used as the prediction targets. All trajectories are transformed into the ego-coordinate system of the 5th frame. The exact formatting protocol is illustrated as follow:

```

1     "conversations": [
2         {
3             "from": "human",
4             "value": "There is last 4frames
5                 trajectory, [PT, [-7.45, 3.05, 0.
6                     16, 0.0, -0.36, 0.93], [-5.7
7                         5, 1.97, 0.11, 0.0, 0.0, -0.28, 0
8                         .96], [-4.04, 0.92, 0.09, 0.0, 0.
9                         0, -0.19, 0.98], [-2.15, 0.26, 0.
10                        04, 0.0, 0.0, -0.1, 1.0]].
11                         Summarize the motion of the ego
12                         vehicle in this 6-frame clip"
13         },
14     ],
15     {
16         "from": "gpt",
17         "value": "[PT, [0.0, 0.0, 0.0, 0.0, 0
18             .0, 0.0, 1.0], [2.47, 0.65, -0.06
19                 , 0.0, 0.0, 0.09, 1.0], [4.24, 2.
20                     32, -0.11, 0.0, 0.0, 0.12, 0.99],
21                     [5.5, 4.08, -0.15, 0.0, 0.0, 0.1
22                         3, 0.99], [7.03, 6.45, -0.15, 0.0
23                         , 0.0, 0.13, 0.99], [8.66, 8.91,
24                         -0.17, -0.01, 0.0, 0.13, 0.99]]"
25     }
26 ]
27 }
```

C. Implementation Details

Our training pipeline consists of three stages. In the first stage, we train the Gaussian tokenizer, projector, and the proposed sampling strategy independently. We then integrate these components with the LLM and perform joint fine-tuning. For the LLM, we adopt a LoRA-based fine-tuning strategy. All models in this stage are trained using 16 NVIDIA A100 GPUs. In the second stage, we train the multi-modal generation module. We start by training a low-resolution (224×400) RGB video generation model, extend it to low-resolution RGB-D generation, and finally refine it into a high-resolution (424×800) RGB-D video generator using a mixed-frame-length strategy. The model is optimized using simulation-free rectified flow and a v-prediction loss [15]. In the final stage, we perform end-to-end joint optimization over all components to ensure consistency between scene understanding and scene generation.

3D Gaussian Scene Loading Strategy. For each processed 3D Gaussian scene, the loading procedure depends on the type of Gaussian features associated with the given QA sample. Since each QA item focuses on a specific keyframe while the number of available camera views varies across scenes, we adopt the following unified strategy:

- **Surround-view Gaussian features.** When the QA sample requires panoramic information, we load the Gaussian

features from all six surrounding views. The Gaussian tokens from all views are concatenated along the token dimension to form a unified set of scene tokens.

- **Single-view Gaussian features.** When the QA sample is associated with a specific camera view, we load only the Gaussian features of that view, without any concatenation.

This design ensures flexibility for different QA formats while maintaining consistent integration of 3D Gaussian scene information into the language model input.

Training Schedule and Parameter Efficiency. During training, the number of epochs is adapted to each task, as the difficulty and convergence behavior differ across region description and perception (RDP), 2D visual grounding (2DVG), 3D visual grounding (3DVG), and planning. Specifically, each task is trained for a task-dependent number of epochs to ensure stable convergence.

In the first-stage training, the number of trainable parameters accounts for only **0.45%** of the total model parameters, focusing mainly on the Gaussian tokenizer, projector, and sampling modules. During the LoRA-based fine-tuning stage, the trainable parameters account for merely **0.79%** of the total model parameters. This demonstrates that our framework achieves strong performance while maintaining high parameter efficiency.

World Knowledge Injection. In our framework, world knowledge is injected into the generative model through a text-conditioned encoder pathway. Specifically, we employ a pretrained language model to convert a natural-language caption into a sequence of semantic tokens, which serve as high-level conditioning signals for the diffusion UNet. Given an input caption, we first tokenize it and encode the sequence using a CLIP-based text encoder. This produces a set of contextualized text embeddings $E_{\text{text}} \in \mathbb{R}^{L \times D}$ where each token represents a semantic unit such as an object category, attribute, or action. Unlike pooled language vectors, which collapse all semantics into a single global descriptor, token-level embeddings preserve fine-grained, word-level structure and allow the diffusion model to selectively attend to relevant parts of the caption. To integrate text knowledge into the generative process, we concatenate the text embeddings with the image-embedding tokens extracted from a reference frame. We further append a learnable type embedding to each token, enabling the model to distinguish between visual and linguistic information during cross-attention. The resulting combined sequence $E_{\text{enc}} = [E_{\text{img}}; E_{\text{text}}] + E_{\text{type}}$ is passed as the encoder-hidden-states to the diffusion UNet, which uses cross-attention at multiple layers to fuse world knowledge with spatial features. Through this mechanism, the UNet learns to associate local visual structures with global textual semantics, enabling the model to leverage descriptions such as object identity, scene context, and commonsense priors to guide novel-

view synthesis. This fusion pathway allows the generative model to incorporate externally grounded world knowledge—captured implicitly by large-scale text–image pre-training of the language encoder—without modifying the underlying UNet architecture. As a result, the model benefits from both low-level geometric cues (RGB/depth latents) and high-level semantic reasoning (text-conditioned cross-attention), improving structural consistency, scene understanding, and semantic controllability during view synthesis.

D. Ablation Study

We additionally provide further ablation studies in Tab. 5, including experiments on the effectiveness of the cross-attention-based sampling module. We also analyse on how world knowledge influences the performance of the generative model in Tab. 7.

E. Extensive Experiments

OmniDrive dataset [46] Scene Understanding Results. We further evaluate our model on the OmniDrive dataset, comparing against strong baselines including GPT-4o [1], LLaVA [32], OmniDrive [46], and Hermes [64]. Our GaussianDWM consistently achieves state-of-the-art performance across all evaluation metrics. These results again confirm the effectiveness of our 3D Gaussian scene representation and task-aware sampling strategy in enhancing LLM-based scene understanding under complex driving scenarios.

We also provide additional qualitative results, including more visualizations of the QA outputs and scene generation results.

Sampling	Gaussian Tokens	2D RD & Pre ↑			2D VG↑			3D VG↑			Plan↑	
		BLEU	Rouge_L	CIDEr	mAP	F1	MIoU	Pr	mAP	F1	Acc	Avg.↑
Top-k + Uniform+Cross	128	68.27	80.95	78.73	34.79	40.3	71.79	51.41	54.01	32.81	68.43	58.15
Top-k + Uniform+Cross	512	68.37	81.00	79.22	34.95	40.39	71.85	51.30	54.07	32.87	68.52	58.26
Top-k + Uniform	4096	66.17	79.07	77.06	33.89	39.31	71.37	51.16	52.87	32.05	66.27	56.92
Top-k + Uniform+Cross	4096	68.20	80.90	78.93	34.50	40.00	71.57	51.20	53.59	32.53	65.60	57.70

Table 5. **Ablation study on Sampling Strategies and Gaussian Token Counts.** We investigate the effectiveness of the proposed Cross-Attention sampling compared to the Uniform baseline. The model with 512 tokens using our strategy achieves the optimal performance, surpassing the dense baseline using 4096 tokens. This indicates that our learned sampling effectively captures critical information with significantly fewer tokens, validating its efficiency.

Model	Reference	# LLM Params	Understanding↑		
			METEOR	ROUGE_L	CIDEr
<i>Only Understanding</i>					
GPT-4o [1]	-	-	-	0.223	0.244
LLaVA-OV [32]	arXiv 24	7B	-	0.221	0.284
OmniDrive [46]	CVPR 25	7B	0.380	0.326	0.686
OmniDrive-2D [46]	CVPR 25	7B	0.383	0.325	0.671
OmniDrive-BEV [46]	CVPR 25	7B	0.356	0.278	0.595
<i>Unified Understanding and Generation</i>					
Separated unification	-	1.8B	0.384	0.327	0.745
HERMES [64]	ICCV 25	1.8B	0.384	0.327	0.741
GaussianDWM	-	8B	0.395	0.341	0.712

Table 6. **OmniDrive dataset [46] Scene Understanding Results.** We further evaluate our model on the OmniDrive dataset, comparing against strong baselines including GPT-4o [1], LLaVA [32], OmniDrive [46], and Hermes [64]. Our GaussianDWM consistently achieves state-of-the-art performance across all evaluation metrics. These results again confirm the effectiveness of our 3D Gaussian scene representation and task-aware sampling strategy in enhancing LLM-based scene understanding under complex driving scenarios.

World Knowledge	Gaussian	shift ± 1m		shift ± 2m		shift ± 4m	
		FID ↓	FVD ↓	FID ↓	FVD ↓	FID ↓	FVD ↓
✗	✗	11.44	42.22	14.75	71.98	21.79	137.31
✓	✗	11.30	41.63	13.96	70.45	19.02	151.19
✓	✓	11.28	41.62	13.95	70.70	18.91	150.05

Table 7. **Ablation on World Knowledge and Gaussian.** We further evaluate the impact of world knowledge by comparing generation model with and without world knowledge, and by examining how Gaussian influences both world knowledge representation and final generation. The improvement brought by world knowledge becomes increasingly significant under larger view shifts. All evaluations are conducted on a subset of 30 scenes from the nuScenes dataset.

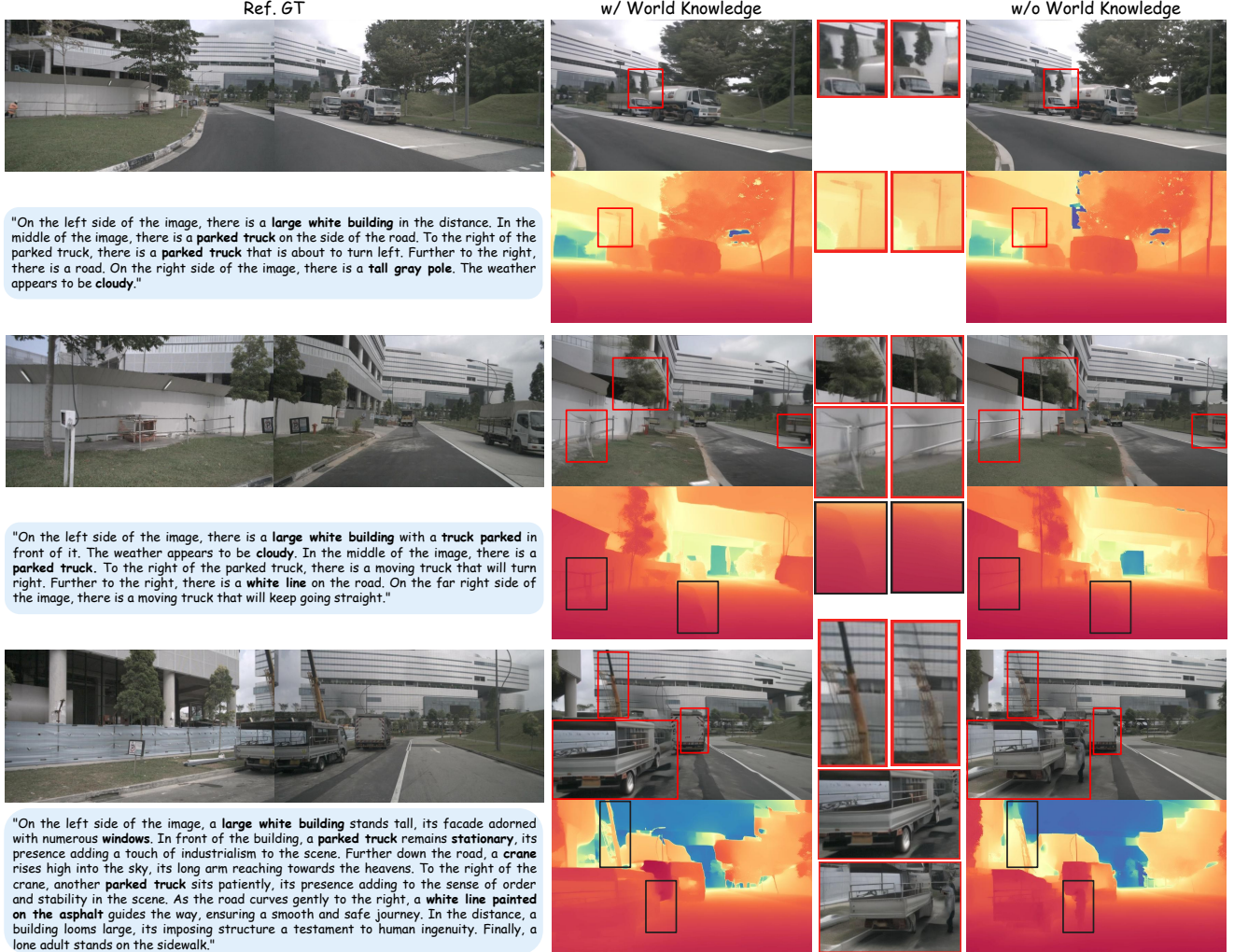


Figure 5. World-Knowledge Ablation. We visualize the effect of world knowledge from LLM under a 4m left-shifted novel view. From left to right: ground-truth images at the original viewpoints (CAM_FRONT and CAM_FRONT_LEFT), world knowledge predicted by our GaussianDWM, novel-view synthesis with world knowledge, and novel-view synthesis without world knowledge. Regions where world knowledge improves semantic and geometric fidelity are highlighted with bounding boxes and zoomed-in at the center. The results show that incorporating world knowledge enables the model to better understand scene context and generate more realistic, semantically consistent geometry.



Q: based on <gauss>, What is the quantity of pedestrian at <CAM_FRONT>, and what are their respective locations? Report bbox coordinates in JSON format.

A: ```json\n[{"bbox_2d": [315, 230, 378, 322], "label": "pedestrian"}]\n```

Q: based on <gauss>, Could you provide the number of car at <CAM_FRONT_RIGHT> and their specific positions? Report bbox coordinates in JSON format.

A: ```json\n[{"bbox_2d": [660, 214, 784, 275], "label": "car"}]\n```

Q: based on <gauss>, Find all pedestrian in this <CAM_FRONT>. For each pedestrian, provide its 3D bounding box. The output format required is JSON: [{"bbox_3d": "x_center, y_center, z_center, x_size, y_size, z_size, roll, pitch, yaw, "label": "category"}]

A: ```json\n[{"bbox_3d": [-1.14, 0.79, 12.17, 0.98, 1.7, 0.74, -0.0, 1.49, 0.98], "label": "pedestrian"}]

Q: based on <gauss>, What approach should the self-vehicle take in this situation?

A: Turn Left.

Q: based on <gauss>, Could you define what the <CAM_FRONT> <box>(315,231),(378,322)</box>, refers to?

A: a adult which is moving.

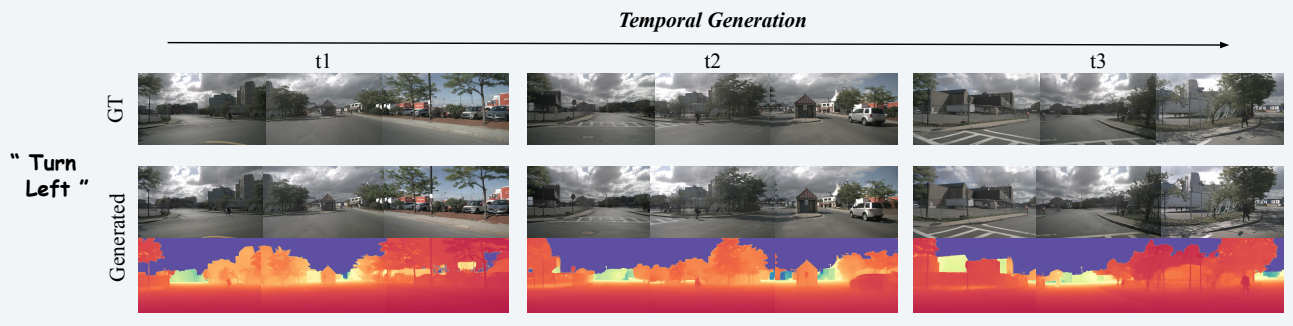
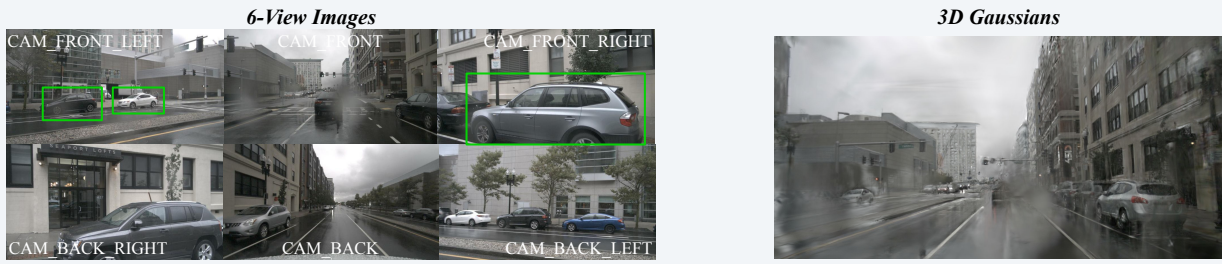


Figure 6. **Qualitative results for scene understanding and scene generation.** From top to bottom, we present the multi-view input of the current scene and the 3D Gaussian ellipsoids, the scene understanding results, and the spatial and temporal scene generation results.



Q: Based on <gauss>, What is the number of car at <CAM_FRONT_LEFT>, and what are their exact positions? Report bbox coordinates in JSON format.

A: ```json\n[\n\t{"bbox_2d": [102, 245, 336, 337], "label": "car"},\n\t{"bbox_2d": [381, 248, 557, 315], "label": "car"}]\n```

Q: Based on <gauss>, Find all car in this <CAM_FRONT_RIGHT>. For each car, provide its 3D bounding box. The output format required is JSON: [{"bbox_3d": {x_center, y_center, z_center, x_size, y_size, z_size, roll, pitch, yaw}, "label": "category"}].

A: [{"bbox_3d": [0.1, 0.71, 4.48, 4.52, 1.63, 1.92, -0.02, 1.8, 0.99], "label": "car"}]

Q: Based on <gauss>, What approach should the self-vehicle take in this situation?

A: Go Straight.

Q: Based on <gauss>, Could you provide a description or explanation of the <CAM_FRONT> <box>(459,240),(489,258)</box>?

A: Parked car.

Q: Based on <gauss>, Can you predict the forthcoming trajectory of the parked car at <CAM_FRONT> <box>(459,240),(489,258)</box>?

A: It will remain stationary.

Q: Based on <gauss>, How might the moving car at <CAM_FRONT> <box>(586,234),(700,267)</box>, dynamically interact with the ego car in its environment?

A: It will be close to the ego car.

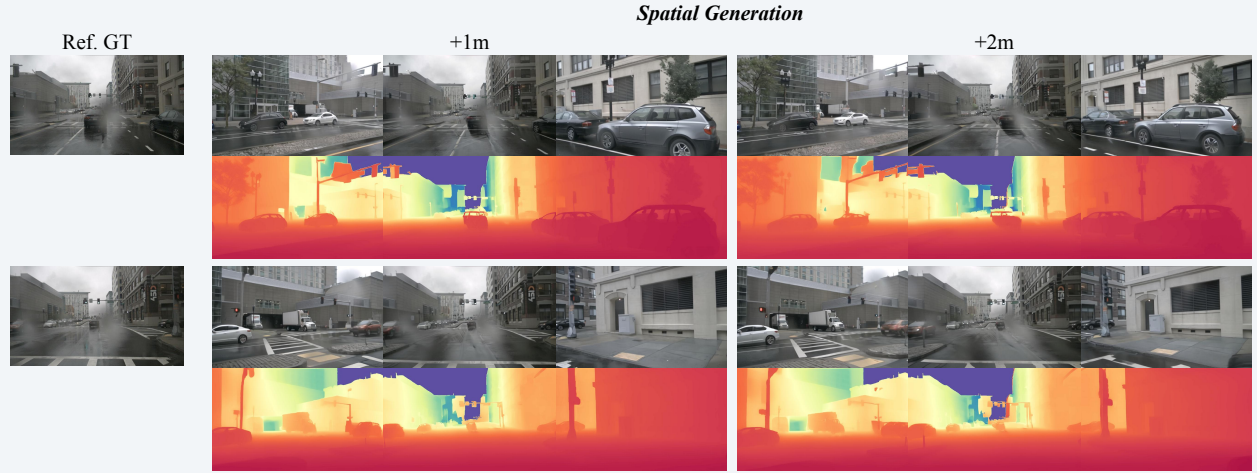
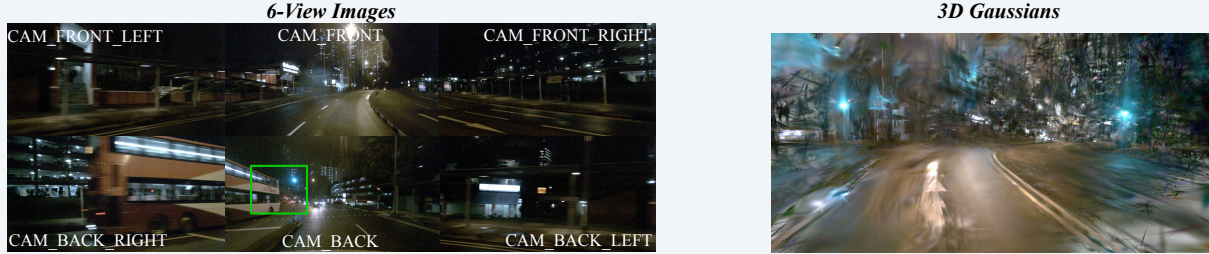


Figure 7. Qualitative results in rainy scene for understanding and generation.



Q: Based on `<gauss>`, What is the count of bus at `<CAM_BACK>`, and what positions do they hold? Report bbox coordinates in JSON format.
A: ``json\n\n\t{\\"bbox_2d\": [275, 230, 297, 261], \\"label\": \\"bus\"\n}''

Q: Based on `<gauss>`, Find all bus in this `<CAM_BACK>`. For each bus, provide its 3D bounding box. The output format required is JSON:
`\{\\"bbox_3d\":\{x_center, y_center, z_center, x_size, y_size, z_size, roll, pitch, yaw\}, \\"label\": \\"category\"\}\}`.
A: [{\\"bbox_3d\": [-20.35, 0.92, 67.75, 12.81, 4.75, 3.29, -0.0, 2.5, 1.0], \\"label\": \\"bus\"\n}]

Q: Based on `<gauss>`, In light of these circumstances, what driving approach is most suitable for the ego car?

A: Turn Right.

Q: Based on `<gauss>`, What the `<CAM_FRONT>` `<box>(743,261),(754,279)</box>` is??
A: Trafficcone.

Q: Based on `<gauss>`, Can you predict the forthcoming trajectory of the trafficcone at `<CAM_FRONT>` `<box>(743,261),(754,279)</box>`?
A: It will remain stationary.

Q: Based on `<gauss>`, What is the spatial relationship between the `<CAM_FRONT_RIGHT>` `<box>(373,0),(784,420)</box>` in relation to the ego vehicle's position?
A: 4.7 meters is the distance from the ego car to it.

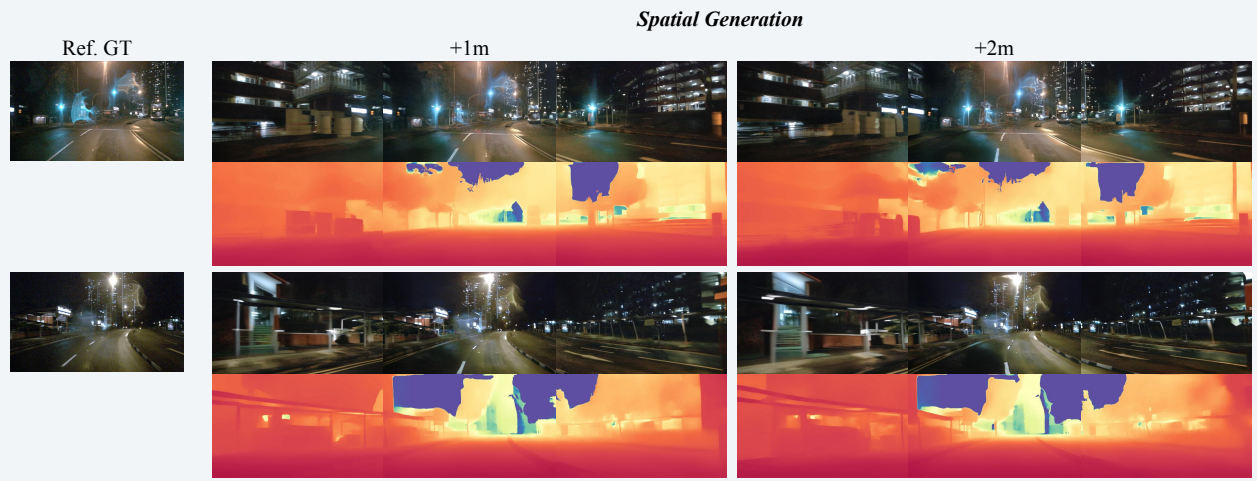


Figure 8. **Qualitative results in nighttime scene for spatial generation and scene understanding.** Our method produces robust and high-quality generation results in both rainy and nighttime conditions.

References

[1] Josh Achiam, Steven Adler, Sandhini Agarwal, Lama Ahmad, Ilge Akkaya, Florencia Leoni Aleman, Diogo Almeida, Janko Altenschmidt, Sam Altman, Shyamal Anadkat, et al. Gpt-4 technical report. *arXiv preprint arXiv:2303.08774*, 2023. 11, 12

[2] Andreas Blattmann, Tim Dockhorn, Sumith Kulal, Daniel Mendelevitch, Maciej Kilian, Dominik Lorenz, Yam Levi, Zion English, Vikram Voleti, Adam Letts, et al. Stable video diffusion: Scaling latent video diffusion models to large datasets. *arXiv preprint arXiv:2311.15127*, 2023. 5

[3] Holger Caesar, Varun Bankiti, Alex H Lang, Sourabh Vora, Venice Erin Liang, Qiang Xu, Anush Krishnan, Yu Pan, Giacarlo Baldan, and Oscar Beijbom. nuscenes: A multi-modal dataset for autonomous driving. In *Proceedings of the IEEE/CVF conference on computer vision and pattern recognition*, pages 11621–11631, 2020. 5, 6, 9

[4] Yurui Chen, Chun Gu, Junzhe Jiang, Xiatian Zhu, and Li Zhang. Periodic vibration gaussian: Dynamic urban scene reconstruction and real-time rendering. *arXiv preprint arXiv:2311.18561*, 2023. 2, 6, 8

[5] Yi Chen, Tianchen Deng, Wentao Zhao, Xiaoning Wang, Wenqian Xi, Weidong Chen, and Jingchuan Wang. Sn-lidar: Semantic neural fields for novel space-time view lidar synthesis. *arXiv preprint arXiv:2504.08361*, 2025. 2

[6] Zhe Chen, Weiyun Wang, Hao Tian, Shenglong Ye, Zhangwei Gao, Erfei Cui, Wenwen Tong, Kongzhi Hu, Jiapeng Luo, Zheng Ma, et al. How far are we to gpt-4v? closing the gap to commercial multimodal models with open-source suites. *Science China Information Sciences*, 67(12):220101, 2024. 5

[7] Ziyu Chen, Jiawei Yang, Jiahui Huang, Riccardo de Lutio, Janick Martinez Esturo, Boris Ivanovic, Or Litany, Zan Gajcic, Sanja Fidler, Marco Pavone, Li Song, and Yue Wang. Omnidre: Omni urban scene reconstruction. In *The Thirteenth International Conference on Learning Representations*, 2025. 6, 8

[8] Tianchen Deng, Siyang Liu, Xuan Wang, Yejia Liu, Danwei Wang, and Weidong Chen. Prosgnerf: Progressive dynamic neural scene graph with frequency modulated auto-encoder in urban scenes. *arXiv preprint arXiv:2312.09076*, 2023. 2

[9] Tianchen Deng, Guole Shen, Tong Qin, Jianyu Wang, Wentao Zhao, Jingchuan Wang, Danwei Wang, and Weidong Chen. Plgslam: Progressive neural scene representation with local to global bundle adjustment. In *Proceedings of the IEEE/CVF Conference on Computer Vision and Pattern Recognition (CVPR)*, pages 19657–19666, 2024. 2

[10] Tianchen Deng, Yue Pan, Shanghai Yuan, Dong Li, Chen Wang, Mingrui Li, Long Chen, Lihua Xie, Danwei Wang, Jingchuan Wang, Javier Civera, Hesheng Wang, and Weidong Chen. What is the best 3d scene representation for robotics? from geometric to foundation models. *arXiv preprint arXiv:2512.03422*, 2025. 3

[11] Tianchen Deng, Guole Shen, Xun Chen, Shanghai Yuan, Hongming Shen, Guohao Peng, Zhenyu Wu, Jingchuan Wang, Lihua Xie, Danwei Wang, Hesheng Wang, and Weidong Chen. Mcn-slam: Multi-agent collaborative neural slam with hybrid implicit neural scene representation. *arXiv preprint arXiv:2506.18678*, 2025. 2

[12] Tianchen Deng, Guole Shen, Chen Xun, Shanghai Yuan, Tongxin Jin, Hongming Shen, Yanbo Wang, Jingchuan Wang, Hesheng Wang, Danwei Wang, et al. Mne-slam: Multi-agent neural slam for mobile robots. In *Proceedings of the Computer Vision and Pattern Recognition Conference*, pages 1485–1494, 2025. 2

[13] Tianchen Deng, Yanbo Wang, Hongle Xie, Hesheng Wang, Rui Guo, Jingchuan Wang, Danwei Wang, and Weidong Chen. Neslam: Neural implicit mapping and self-supervised feature tracking with depth completion and denoising. *IEEE Transactions on Automation Science and Engineering*, 22: 12309–12321, 2025. 2

[14] Tianchen Deng, Wenhua Wu, Junjie He, Yue Pan, Xirui Jiang, Shanghai Yuan, Danwei Wang, Hesheng Wang, and Weidong Chen. Vpgs-slam: Voxel-based progressive 3d gaussian slam in large-scale scenes. *arXiv preprint arXiv:2505.18992*, 2025. 2

[15] Patrick Esser, Sumith Kulal, Andreas Blattmann, Rahim Entezari, Jonas Müller, Harry Saini, Yam Levi, Dominik Lorenz, Axel Sauer, Frederic Boesel, et al. Scaling rectified flow transformers for high-resolution image synthesis. In *Forty-first international conference on machine learning*, 2024. 5, 10

[16] Ruiyuan Gao, Kai Chen, Enze Xie, Lanqing Hong, Zhenguo Li, Dit-Yan Yeung, and Qiang Xu. Magicdrive: Street view generation with diverse 3d geometry control. *arXiv preprint arXiv:2310.02601*, 2023. 3, 6

[17] Shenyuan Gao, Jiazheng Yang, Li Chen, Kashyap Chitta, Yihang Qiu, Andreas Geiger, Jun Zhang, and Hongyang Li. Vista: A generalizable driving world model with high fidelity and versatile controllability. *Advances in Neural Information Processing Systems*, 37:91560–91596, 2024. 2

[18] Ruocheng Gu, Sen Jia, Yule Ma, Jinjin Zhong, Jenq-Neng Hwang, and Lei Li. Mocount: Motion-based repetitive action counting. In *Proceedings of the 33rd ACM International Conference on Multimedia*, pages 9026–9034, 2025. 2

[19] Jiazhe Guo, Yikang Ding, Xiwu Chen, Shuo Chen, Bohan Li, Yingshuang Zou, Xiaoyang Lyu, Feiyang Tan, Xiaojuan Qi, Zhiheng Li, and Hao Zhao. Dist-4d: Disentangled spatiotemporal diffusion with metric depth for 4d driving scene generation. In *Proceedings of the IEEE/CVF International Conference on Computer Vision (ICCV)*, page 27231–27241, 2025. 6

[20] Jiazhe Guo, Yikang Ding, Xiwu Chen, Shuo Chen, Bohan Li, Yingshuang Zou, Xiaoyang Lyu, Feiyang Tan, Xiaojuan Qi, Zhiheng Li, et al. Dist-4d: Disentangled spatiotemporal diffusion with metric depth for 4d driving scene generation. *arXiv preprint arXiv:2503.15208*, 2025. 2, 6

[21] Anna-Maria Halacheva, Jan-Nico Zaech, Xi Wang, Danda Pani Paudel, and Luc Van Gool. Gaussianvilm: Scene-centric 3d vision-language models using language-aligned gaussian splats for embodied reasoning and beyond. *arXiv preprint arXiv:2507.00886*, 2025. 3

[22] Yining Hong, Haoyu Zhen, Peihao Chen, Shuhong Zheng, Yilun Du, Zhenfang Chen, and Chuang Gan. 3d-ilm: Injecting the 3d world into large language models. *Advances*

in Neural Information Processing Systems, 36:20482–20494, 2023. 3

[23] Anthony Hu, Lloyd Russell, Hudson Yeo, Zak Murez, George Fedoseev, Alex Kendall, Jamie Shotton, and Gianluca Corrado. Gaia-1: A generative world model for autonomous driving. *arXiv preprint arXiv:2309.17080*, 2023. 2

[24] Anthony Hu, Lloyd Russell, Hudson Yeo, Zak Murez, George Fedoseev, Alex Kendall, Jamie Shotton, and Gianluca Corrado. Gaia-1: A generative world model for autonomous driving. *arXiv preprint arXiv:2309.17080*, 2023. 2

[25] Bernhard Kerbl, Georgios Kopanas, Thomas Leimkühler, and George Drettakis. 3d gaussian splatting for real-time radiance field rendering. *ACM Trans. Graph.*, 42(4):139–1, 2023. 2

[26] Alexander Kirillov, Eric Mintun, Nikhila Ravi, Hanzi Mao, Chloe Rolland, Laura Gustafson, Tete Xiao, Spencer Whitehead, Alexander C Berg, Wan-Yen Lo, et al. Segment anything. In *Proceedings of the IEEE/CVF international conference on computer vision*, pages 4015–4026, 2023. 3, 9

[27] Lingdong Kong, Wesley Yang, Jianbiao Mei, Youquan Liu, Ao Liang, Dekai Zhu, Dongyue Lu, Wei Yin, Xiaotao Hu, Mingkai Jia, et al. 3d and 4d world modeling: A survey. *arXiv preprint arXiv:2509.07996*, 2025. 2

[28] Bohan Li, Jiazhe Guo, Hongsi Liu, Yingshuang Zou, Yikang Ding, Xiwu Chen, Hu Zhu, Feiyang Tan, Chi Zhang, Tiancai Wang, et al. Uniscene: Unified occupancy-centric driving scene generation. In *Proceedings of the Computer Vision and Pattern Recognition Conference*, pages 11971–11981, 2025. 3

[29] Lei Li, Sen Jia, Jianhao Wang, Zhongyu Jiang, Feng Zhou, Ju Dai, Tianfang Zhang, Zongkai Wu, and Jenq-Neng Hwang. Human motion instruction tuning. In *Proceedings of the Computer Vision and Pattern Recognition Conference*, pages 17582–17591, 2025. 2

[30] Zhiqi Li, Wenhui Wang, Hongyang Li, Enze Xie, Chong-hao Sima, Tong Lu, Qiao Yu, and Jifeng Dai. Bevformer: learning bird’s-eye-view representation from lidar-camera via spatiotemporal transformers. *IEEE Transactions on Pattern Analysis and Machine Intelligence*, 2024. 5

[31] Chin-Yew Lin. Rouge: A package for automatic evaluation of summaries. In *Text summarization branches out*, pages 74–81, 2004. 5

[32] Haotian Liu, Chunyuan Li, Yuheng Li, and Yong Jae Lee. Improved baselines with visual instruction tuning. In *Proceedings of the IEEE/CVF conference on computer vision and pattern recognition*, pages 26296–26306, 2024. 5, 11, 12

[33] Yingfei Liu, Tiancai Wang, Xiangyu Zhang, and Jian Sun. Petr: Position embedding transformation for multi-view 3d object detection. In *European conference on computer vision*, pages 531–548. Springer, 2022. 5

[34] Jiageng Mao, Boyi Li, Boris Ivanovic, Yuxiao Chen, Yan Wang, Yurong You, Chaowei Xiao, Danfei Xu, Marco Pavone, and Yue Wang. Dreamdrive: Generative 4d scene modeling from street view images. In *2025 IEEE International Conference on Robotics and Automation (ICRA)*, pages 367–374. IEEE, 2025. 3

[35] Ben Mildenhall, Pratul P Srinivasan, Matthew Tancik, Jonathan T Barron, Ravi Ramamoorthi, and Ren Ng. Nerf: Representing scenes as neural radiance fields for view synthesis. *Communications of the ACM*, 65(1):99–106, 2021. 2, 3

[36] Julian Ost, Fahim Mannan, Nils Thuerey, Julian Knodt, and Felix Heide. Neural scene graphs for dynamic scenes. In *Proceedings of the IEEE/CVF Conference on Computer Vision and Pattern Recognition*, pages 2856–2865, 2021. 2

[37] Kishore Papineni, Salim Roukos, Todd Ward, and Wei-Jing Zhu. Bleu: a method for automatic evaluation of machine translation. In *Proceedings of the 40th annual meeting of the Association for Computational Linguistics*, pages 311–318, 2002. 5

[38] Chensheng Peng, Ido Sobol, Masayoshi Tomizuka, Kurt Keutzer, Chenfeng Xu, and Or Litany. A lesson in splats: Teacher-guided diffusion for 3d gaussian splats generation with 2d supervision. In *Proceedings of the IEEE/CVF International Conference on Computer Vision*, pages 28707–28717, 2025. 2

[39] Chensheng Peng, Chengwei Zhang, Yixiao Wang, Chenfeng Xu, Yichen Xie, Wenzhao Zheng, Kurt Keutzer, Masayoshi Tomizuka, and Wei Zhan. Desire-gs: 4d street gaussians for static-dynamic decomposition and surface reconstruction for urban driving scenes. In *Proceedings of the IEEE/CVF Conference on Computer Vision and Pattern Recognition (CVPR)*, pages 6782–6791, 2025. 2

[40] Minghan Qin, Wanhua Li, Jiawei Zhou, Haoqian Wang, and Hanspeter Pfister. Langsplat: 3d language gaussian splatting. In *Proceedings of the IEEE/CVF Conference on Computer Vision and Pattern Recognition*, pages 20051–20060, 2024. 3, 9

[41] Chonghao Sima, Katrin Renz, Kashyap Chitta, Li Chen, Hanxue Zhang, Chengan Xie, Jens Beißwenger, Ping Luo, Andreas Geiger, and Hongyang Li. Drivelm: Driving with graph visual question answering. In *European conference on computer vision*, pages 256–274. Springer, 2024. 3

[42] Qijian Tian, Xin Tan, Yuan Xie, and Lizhuang Ma. Drivingforward: Feed-forward 3d gaussian splatting for driving scene reconstruction from flexible surround-view input. In *Proceedings of the AAAI Conference on Artificial Intelligence*, pages 7374–7382, 2025. 2

[43] Haithem Turki, Jason Y Zhang, Francesco Ferroni, and Deva Ramanan. Suds: Scalable urban dynamic scenes. In *Proceedings of the IEEE/CVF Conference on Computer Vision and Pattern Recognition*, pages 12375–12385, 2023. 2

[44] Ramakrishna Vedantam, C Lawrence Zitnick, and Devi Parikh. Cider: Consensus-based image description evaluation. In *Proceedings of the IEEE conference on computer vision and pattern recognition*, pages 4566–4575, 2015. 5

[45] Qitai Wang, Lue Fan, Yuqi Wang, Yuntao Chen, and Zhaoxiang Zhang. Freevs: Generative view synthesis on free driving trajectory. In *Proceedings of the International Conference on Learning Representations (ICLR)*, 2025. 6

[46] Shihao Wang, Zhiding Yu, Xiaohui Jiang, Shiyi Lan, Min Shi, Nadine Chang, Jan Kautz, Ying Li, and Jose M Al

varez. Omnidrive: A holistic vision-language dataset for autonomous driving with counterfactual reasoning. In *Proceedings of the Computer Vision and Pattern Recognition Conference*, pages 22442–22452, 2025. 11, 12

[47] Yuqi Wang, Jiawei He, Lue Fan, Hongxin Li, Yuntao Chen, and Zhaoxiang Zhang. Driving into the future: Multiview visual forecasting and planning with world model for autonomous driving. In *Proceedings of the IEEE/CVF Conference on Computer Vision and Pattern Recognition*, pages 14749–14759, 2024. 2

[48] Yanbo Wang, Zipeng Fang, Lei Zhao, and Weidong Chen. Learning to tune like an expert: Interpretable and scene-aware navigation via mllm reasoning and cvae-based adaptation. *arXiv preprint arXiv:2507.11001*, 2025. 3

[49] Yue Wen, Liang Song, Yijia Liu, Siting Zhu, Yanzi Miao, Lijun Han, and Hesheng Wang. Freedriverf: Monocular rgb dynamic nerf without poses for autonomous driving via point-level dynamic-static decoupling. *arXiv preprint arXiv:2505.09406*, 2025. 2

[50] Jinbo Xing, Menghan Xia, Yong Zhang, Haoxin Chen, Wangbo Yu, Hanyuan Liu, Gongye Liu, Xintao Wang, Ying Shan, and Tien-Tsin Wong. Dynamicrafter: Animating open-domain images with video diffusion priors. In *European Conference on Computer Vision*, pages 399–417. Springer, 2024. 5

[51] Kaixin Xiong, Shi Gong, Xiaoqing Ye, Xiao Tan, Ji Wan, Errui Ding, Jingdong Wang, and Xiang Bai. Cape: Camera view position embedding for multi-view 3d object detection. In *Proceedings of the IEEE/CVF conference on computer vision and pattern recognition*, pages 21570–21579, 2023. 5

[52] Zhenhua Xu, Yujia Zhang, Enze Xie, Zhen Zhao, Yong Guo, Kwan-Yee K Wong, Zhenguo Li, and Hengshuang Zhao. Drivegpt4: Interpretable end-to-end autonomous driving via large language model. *IEEE Robotics and Automation Letters*, 2024. 3

[53] Tianyi Yan, Dongming Wu, Wencheng Han, Junpeng Jiang, Xia Zhou, Kun Zhan, Cheng-zhong Xu, and Jianbing Shen. Drivingsphere: Building a high-fidelity 4d world for closed-loop simulation. In *Proceedings of the Computer Vision and Pattern Recognition Conference*, pages 27531–27541, 2025. 2

[54] Yunzhi Yan, Haotong Lin, Chenxu Zhou, Weijie Wang, Haiyang Sun, Kun Zhan, Xianpeng Lang, Xiaowei Zhou, and Sida Peng. Street gaussians: Modeling dynamic urban scenes with gaussian splatting. In *European Conference on Computer Vision*, pages 156–173. Springer, 2024. 2, 6, 8

[55] An Yang, Anfeng Li, Baosong Yang, Beichen Zhang, Binyuan Hui, Bo Zheng, Bowen Yu, Chang Gao, Chengan Huang, Chenxu Lv, et al. Qwen3 technical report. *arXiv preprint arXiv:2505.09388*, 2025. 2, 4

[56] Jiawei Yang, Boris Ivanovic, Or Litany, Xinshuo Weng, Seung Wook Kim, Boyi Li, Tong Che, Danfei Xu, Sanja Fidler, Marco Pavone, et al. Emernerf: Emergent spatial-temporal scene decomposition via self-supervision. *arXiv preprint arXiv:2311.02077*, 2023. 2, 6

[57] Jiawei Yang, Jiahui Huang, Yuxiao Chen, Yan Wang, Boyi Li, Yurong You, Apoorva Sharma, Maximilian Igl, Peter Karkus, Danfei Xu, et al. Storm: Spatio-temporal reconstruction model for large-scale outdoor scenes. *arXiv preprint arXiv:2501.00602*, 2024. 2

[58] Ziyi Yang, Xinyu Gao, Wen Zhou, Shaohui Jiao, Yuqing Zhang, and Xiaogang Jin. Deformable 3d gaussians for high-fidelity monocular dynamic scene reconstruction. *arXiv preprint arXiv:2309.13101*, 2023. 8

[59] Zetong Yang, Li Chen, Yanan Sun, and Hongyang Li. Visual point cloud forecasting enables scalable autonomous driving. In *Proceedings of the IEEE/CVF Conference on Computer Vision and Pattern Recognition*, pages 14673–14684, 2024. 2

[60] Guosheng Zhao, Xiaofeng Wang, Zheng Zhu, Xinze Chen, Guan Huang, Xiaoyi Bao, and Xingang Wang. Drivedreamer-2: Llm-enhanced world models for diverse driving video generation. In *Proceedings of the AAAI Conference on Artificial Intelligence*, pages 10412–10420, 2025. 2

[61] Zongchuang Zhao, Haoyu Fu, Dingkang Liang, Xin Zhou, Dingyuan Zhang, Hongwei Xie, Bing Wang, and Xiang Bai. Extending large vision-language model for diverse interactive tasks in autonomous driving. *arXiv preprint arXiv:2505.08725*, 2025. 3, 5, 6

[62] Haoyu Zhen, Xiaowen Qiu, Peihao Chen, Jincheng Yang, Xin Yan, Yilun Du, Yining Hong, and Chuang Gan. 3d-vla: A 3d vision-language-action generative world model. *arXiv preprint arXiv:2403.09631*, 2024. 3

[63] Xiaoyu Zhou, Zhiwei Lin, Xiaojun Shan, Yongtao Wang, Deqing Sun, and Ming-Hsuan Yang. Drivinggaussian: Composite gaussian splatting for surrounding dynamic autonomous driving scenes. In *Proceedings of the IEEE/CVF conference on computer vision and pattern recognition*, pages 21634–21643, 2024. 2

[64] Xin Zhou, Dingkang Liang, Sifan Tu, Xiwu Chen, Yikang Ding, Dingyuan Zhang, Feiyang Tan, Hengshuang Zhao, and Xiang Bai. Hermes: A unified self-driving world model for simultaneous 3d scene understanding and generation. *arXiv preprint arXiv:2501.14729*, 2025. 2, 3, 11, 12

[65] Yingshuang Zou, Yikang Ding, Chuanrui Zhang, Jiazhe Guo, Bohan Li, Xiaoyang Lyu, Feiyang Tan, Xiaojuan Qi, and Haoqian Wang. Mudg: Taming multi-modal diffusion with gaussian splatting for urban scene reconstruction. *arXiv preprint arXiv:2503.10604*, 2025. 2